Full Wave Analysis of Edge-Guided Mode Microstrip Isolator

Tarief M. F. Elshafiey, *Student Member, IEEE,* James T. Aberle, *Senior Member, IEEE,* and El-Badawy El-Sharawy, *Senior Member, IEEE*

***Abstract*— This paper presents a full-wave analysis of three edge-guided mode microstrip isolator structures. Galerkin's technique in the spectral domain is used to calculate the insertion loss and the isolation of the structures. The paper presents figures of merit of different multilayer structures. A multilayer structure resulted in increased isolation and lower insertion loss.**

I. Introduction

THE edge-isolator is one of the most widely used magnetic devices. The principle of operation of these devices is based on the field displacement effect, i.e., the microwave field configurations of the forward and backward propagating waves are different. If an absorbing resistive film is placed at one edge of the conductor, then different attenuation of these two waves occurs and an isolator is realized. The geometry of an isolator with a resistive thin film is shown in Fig. 1. Experimental work on this type of isolator has been widely reported in the literature [1]–[7]. Approximate theoretical analyzes have also been reported [8]–[10]. However, no full-wave analysis of the present structure has been reported to date.

II. Full Wave Formulation

A versatile technique for formulating the Green's function for structures with transversely magnetized ferrite substrates was first described by El-Sharawy [1]. This technique utilizes the transmission matrix of the ferrite layer, wherein all the fields are expressed in terms of arbitrary constants that arise in the solution of the wave equation of the medium. The same technique is used here to derive the Green's function for structures containing a normally magnetized ferrite substrate. The transmission matrix $\overline{\overline{\tilde{T}}}$ is a 4×4 matrix written as [11]

$$\begin{bmatrix} \overline{\tilde{E}}_2 \\ \overline{\tilde{J}}_2 \end{bmatrix} = \overline{\overline{\tilde{T}}} \begin{bmatrix} \overline{\tilde{E}}_1 \\ \overline{\tilde{J}}_1 \end{bmatrix} = \begin{bmatrix} \overline{\overline{\tilde{T}}}^E & \overline{\tilde{Z}}^T \\ \overline{\tilde{Y}}^T & \overline{\overline{\tilde{T}}}^J \end{bmatrix} \begin{bmatrix} \overline{\tilde{E}}_1 \\ \overline{\tilde{J}}_1 \end{bmatrix} \tag{1}$$

where $\overline{\overline{\tilde{T}}}^E, \overline{\tilde{Z}}^T, \overline{\tilde{Y}}^T, \overline{\overline{\tilde{T}}}^J$ are 2×2 submatrices of $\overline{\overline{\tilde{T}}}$, "$\sim$" denotes the spatial Fourier transform defined as

$$\overline{\tilde{E}}(K_x, K_y) = \int_{-\infty}^{\infty} \int_{-\infty}^{\infty} \overline{E}(x, y) e^{-jK_x x} e^{-jK_y y}\, dx\, dy \tag{2}$$

$\overline{\tilde{E}}_1$ and $\overline{\tilde{E}}_2$ are the tangential electric field at the boundaries of the layer and $\overline{\tilde{J}}_1$ and $\overline{\tilde{J}}_2$ are the tangential surface currents defined by $\overline{\tilde{J}}_n = \hat{z} \times \overline{\tilde{H}}_n$, where $\overline{\tilde{H}}_n$ is the tangential magnetic field at the nth surface of the layer.

Because of the nature of the problem, the normally biased ferrite substrate transmission matrix is more difficult to derive than the one for transversely biased ferrite. The derivation was greatly facilitated by the use of the symbolic computation software, MAPLE V [12].

We investigated three different isolator structures. The first structure comprises a single normally magnetized ferrite substrate as shown in Fig. 2. In the second structure, we added another dielectric layer underneath the ferrite layer as shown in Fig. 3. The third structure, called "drop-in element," is an isolator structure compatible with Monolithic Microwave Integrated Circuits (MMIC). In this structure, a dielectric substrate with relative permittivity equal to 9.8 is used. To form an EG isolator, we place a piece of ferrite with a resistive thin film on top of the dielectric as shown in Fig. 4.

A. Green's Function Formulation

A spectral-domain Green's function, $\overline{\overline{\tilde{G}}}$, is formulated that relates the transformed electric field $\overline{\tilde{E}}_s$ on one surface to the transformed electric surface currents $\overline{\tilde{J}}_s$, on the same surface. This relation has the form

$$\overline{\tilde{E}}_s(k_x, k_y) = \overline{\overline{\tilde{G}}}(k_x, k_y) \overline{\tilde{J}}_s(k_x, k_y). \tag{3}$$

Using the transmission matrix, Green's functions can be formulated in the spectral domain for single and multilayer structures. For the single-layer structure, the Green's function is

$$\overline{\overline{\tilde{G}}} = (\overline{\overline{\tilde{T}}}_f^J \overline{\tilde{Z}}_f^{T-1} + \overline{\overline{\tilde{G}}}_a^{-1})^{-1} \tag{4}$$

where $\overline{\tilde{Z}}_f^T$ and $\overline{\overline{\tilde{T}}}_f^J$ are submatrices of the transmission matrix of a normally biased ferrite layer and $\overline{\overline{\tilde{G}}}_a$ is a semispace Green's function, which is calculated by taking the limit of the dielectric Green's function when the thicknes of the layer d_d goes to infinity and the dielectric constant goes to one

$$\overline{\overline{\tilde{G}}}_a = \lim_{\substack{d_d \to \infty \\ \epsilon_d \to 1}} \overline{\overline{\tilde{G}}}_d \tag{5}$$

where $\overline{\overline{\tilde{G}}}_d$ is formed using the dielectric transmission matrix derived by El-Sharawy [11].

For the ferrite-dielectric structure, the Green's function is

$$\overline{\overline{\tilde{G}}} = (\overline{\overline{\tilde{T}}}^J \overline{\tilde{Z}}^{T-1} + \overline{\overline{\tilde{G}}}_a^{-1})^{-1} \tag{6}$$

Manuscript received April 1, 1996.

The authors are with the Telecommunications Research Center, Arizona State University, Tempe, AZ 85287 USA.

Publisher Item Identifier S 0018-9480(96)08562-6.

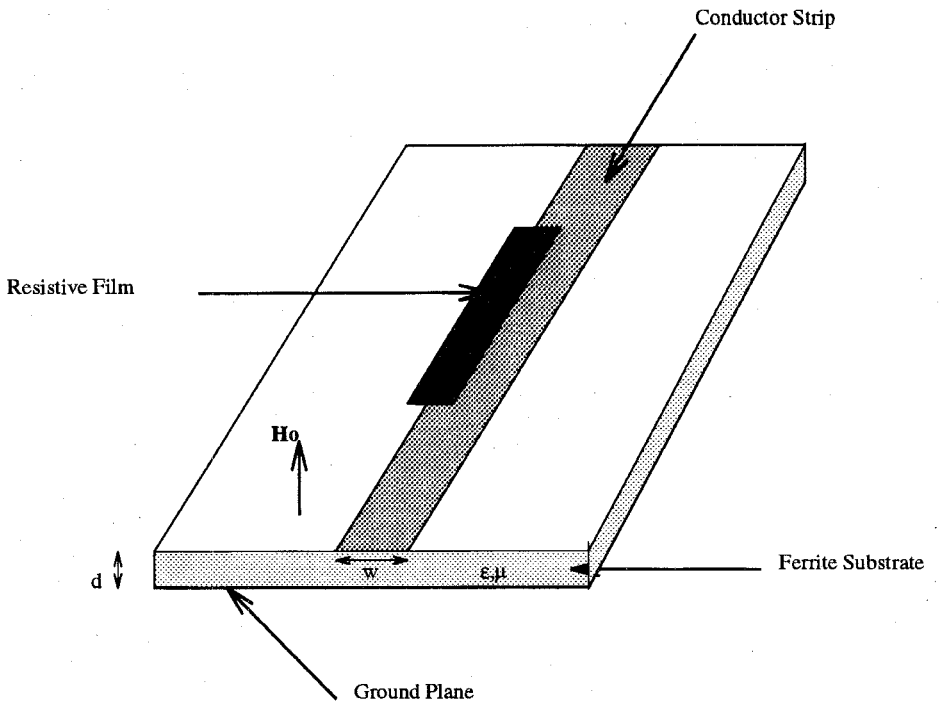

Fig. 1. Edge-guided isolator with resistive film loading.

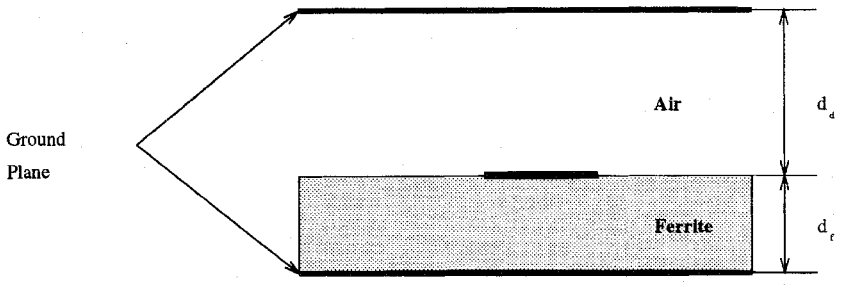

Fig. 2. Geometry of single layer structure.

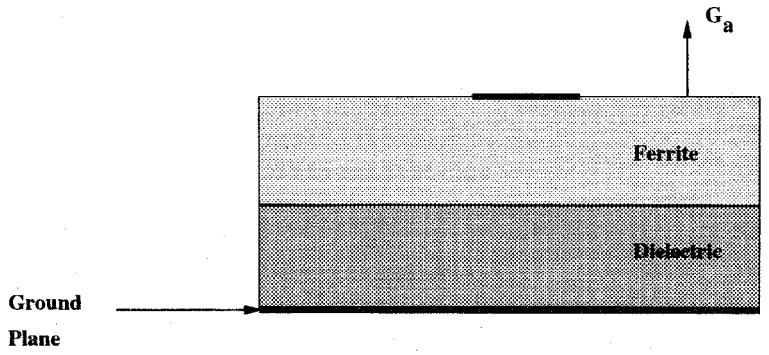

Fig. 3. Geometry of double layer structure.

and $\overline{\tilde{Z}}^T$ and $\overline{\tilde{T}}^J$ are the elements of $[T_{\text{new}}]$ where

$$[\tilde{T}_{\text{new}}] = [\tilde{T}_f][\tilde{T}_d]$$

which is the result of the ferrite and dielectric transmission matrix multiplication.

For the three layer structure (the drop-in element) the Green's function is

$$\overline{\overline{\tilde{G}}} = (\overline{\tilde{T}}_u^J \overline{\tilde{Z}}_u^{T-1} + \overline{\tilde{T}}_d^J \overline{\tilde{Z}}_d^{T-1})^{-1} \tag{7}$$

where $\overline{\tilde{Z}}_u^T$ and $\overline{\tilde{T}}_u^J$ are the elements of the new transmission matrix which resulted from the ferrite and air transmission matrix multiplication.

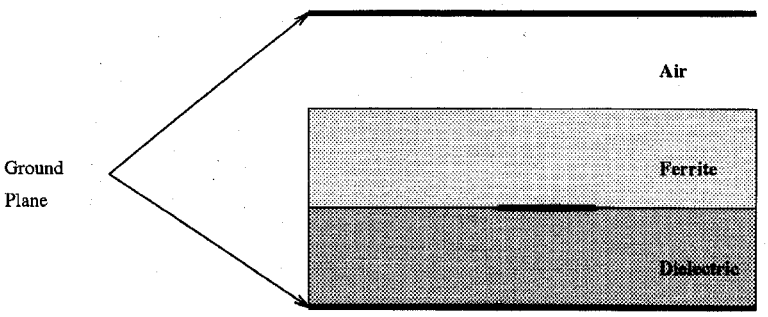

Fig. 4. Geometry of drop-in element structure.

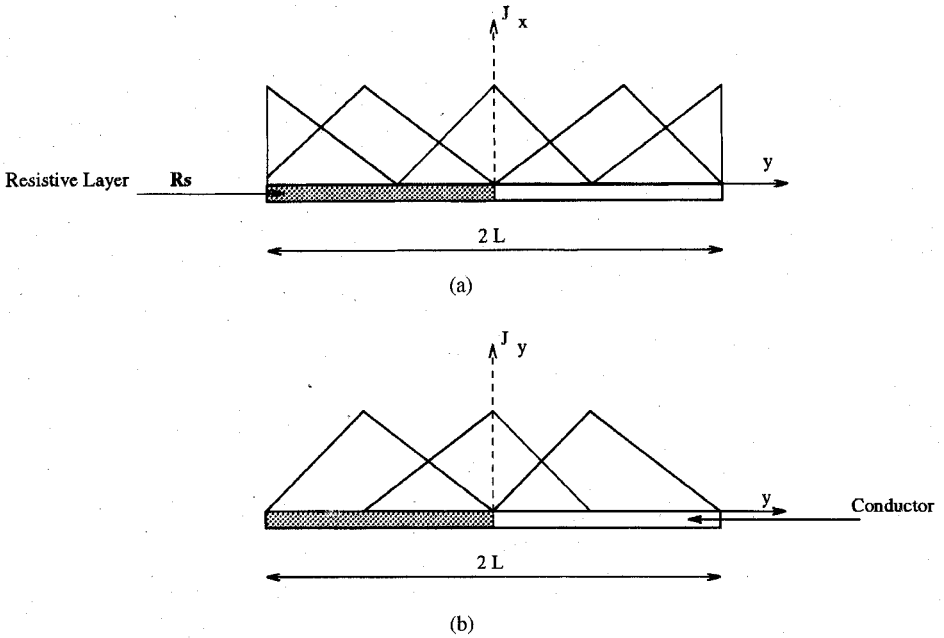

Fig. 5. Current basis functions for (a) longitudinal current (b) transverse current.

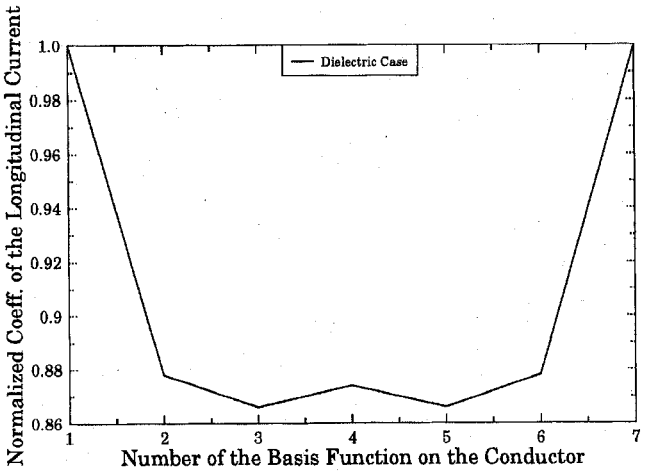

Fig. 6. Symmetric current distribution over dielectric microstrip.

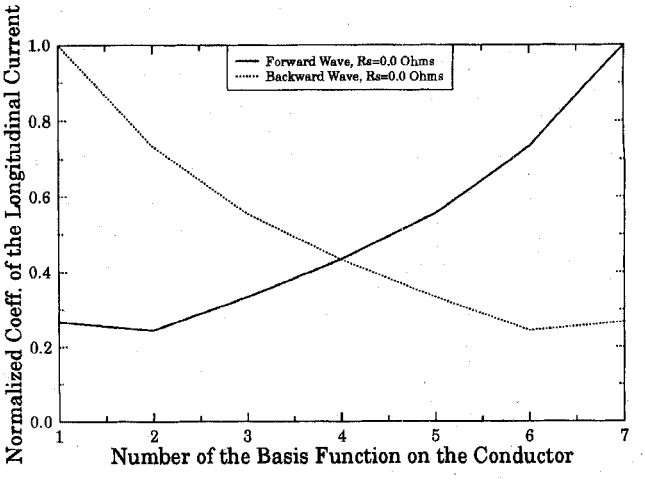

Fig. 7. Asymmetric current over ferrite microstrip in forward and backward directions for $R_s = 0$.

B. Basis Functions and Resistive Region Treatment

We selected piece-wise linear basis functions to represent the current on the microstrip as shown in Fig. 5. The current in y-direction (transverse) is zero at the edges of the conductor and the current in x-direction (longitudinal) is maximum at the edges to satisfy the edge conditions.

Five basis functions in y-direction and seven basis functions in x-direction are found to be sufficient for convergence of the solution. In matrix notation, the system matrix can be written as

$$\begin{bmatrix} \tilde{E}_x \\ \tilde{E}_y \end{bmatrix} = \left[\begin{bmatrix} \tilde{Z}_{xx} & \tilde{Z}_{xy} \\ \tilde{Z}_{yx} & \tilde{Z}_{yy} \end{bmatrix} + \begin{bmatrix} R_{xx} & 0 \\ 0 & R_{yy} \end{bmatrix} \right] \begin{bmatrix} \tilde{J}_x \\ \tilde{J}_y \end{bmatrix}. \quad (8)$$

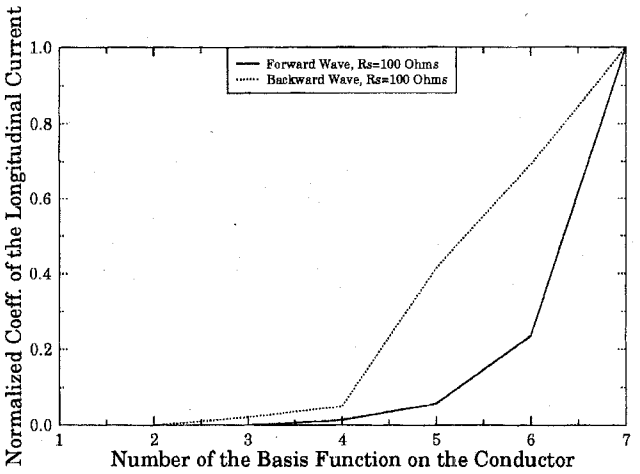

Fig. 8. Asymmetric current over ferrite microstrip in forward and backward directions for $R_s = 100\ \Omega$.

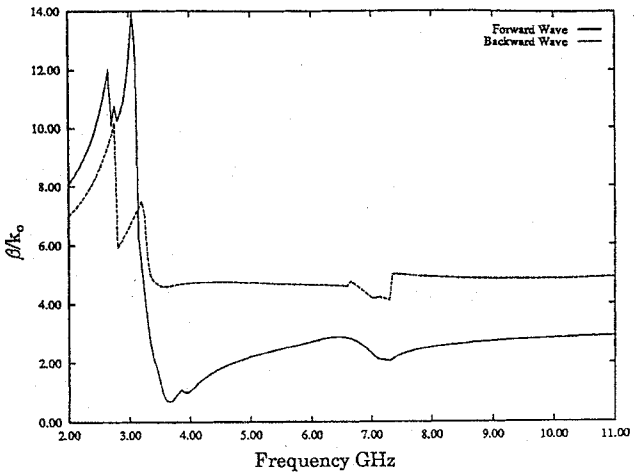

Fig. 9. The phase constants of forward and backward waves ($d = 7.62 \times 10^{-4}$ m, $\epsilon_f = 12.0, 4\pi M_s = 1750$ G, $H_{dc} = 800Oe, \Delta H = 80.$ Oe, $R_s = 100\ \Omega, W = 1.016 \times 10^{-2}$ m).

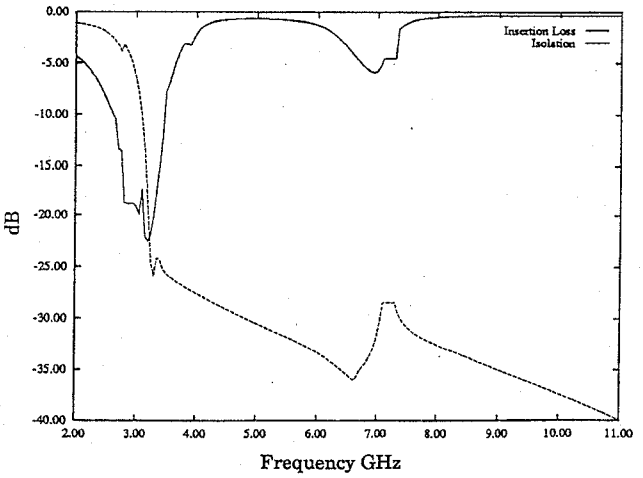

Fig. 10. Computed isolation and insertion loss ($d = 7.62 \times 10^{-4}$ m, $\epsilon_f = 12.0, 4\pi M_s = 1750$ G, $H_{dc} = 800$ Oe, $\Delta H = 80.$ Oe, $R_s = 100\ \Omega, W = 1.016 \times 10^{-2}$ m).

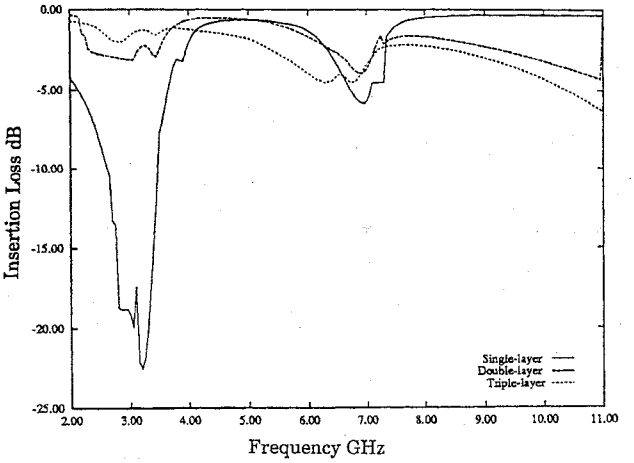

Fig. 11. Comparison of the insertion loss for three isolator structures. ($4\pi M_s = 1750$ G, $H_{dc} = 800$ Oe, $\Delta H = 80.$ Oe, $R_s = 100\ \Omega, W = 1.016E-2$ m. For the single-layer: $d_f = 7.62E-04$ m, $\epsilon_f = 12.0$. For the double-layer: $d_d = 2.62E-04$ m, $\epsilon_d = 3.00$. For the triple-layer: $d_d = 4.00E-04$ m, $\epsilon_d = 8.90 d_a = 5.00E-03$ m, $\epsilon_a = 1.00$).

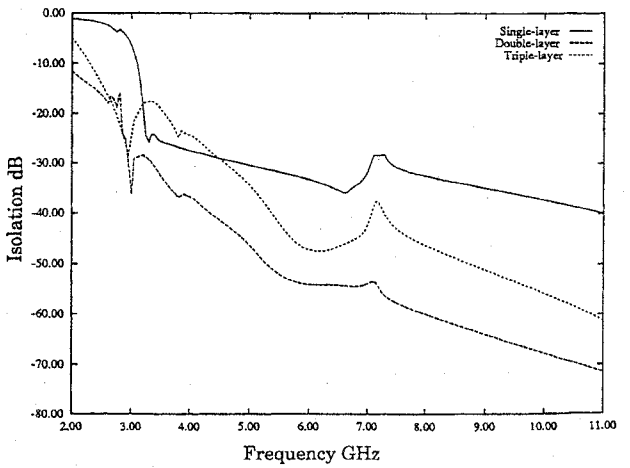

Fig. 12. Comparison of the isolation for three isolator structures. ($4\pi M_s = 1750$ G, $H_{dc} = 800$ Oe, $\Delta H = 80.$ Oe, $R_s = 100\ \Omega, W = 1.016E-2$ m. For the single-layer: $d_f = 7.62E-04$ m, $\epsilon_f = 12.0$. For the double-layer: $d_d = 2.62E-04$ m, $\epsilon_d = 3.00$. For the triple-layer: $d_d = 4.00E-04$ m, $\epsilon_d = 8.90\ d_a = 5.00E-03$ m, $\epsilon_a = 1.00$).

We separate the resistive matrix from the impedance matrix, and integrate the resistive matrix in spatial domain in closed form once. We also exploit the block Toeplitz symmetry of the impedance matrix. This means that only the first two rows and the first two columns of each submatrix must be calculated. The remaining terms of each submatrix can be filled by using the terms of the first two rows and first two columns, thus reducing the time needed to calculate the impedance matrix.

C. Numerical Considerations in the Evaluation of the Spectral Domain Integration

The spectral domain integrals required in the evaluation of the impedance matrix elements are evaluated numerically using sixteen-point gaussian quadrature. The numerical integration must be carried out to a sufficiently large number

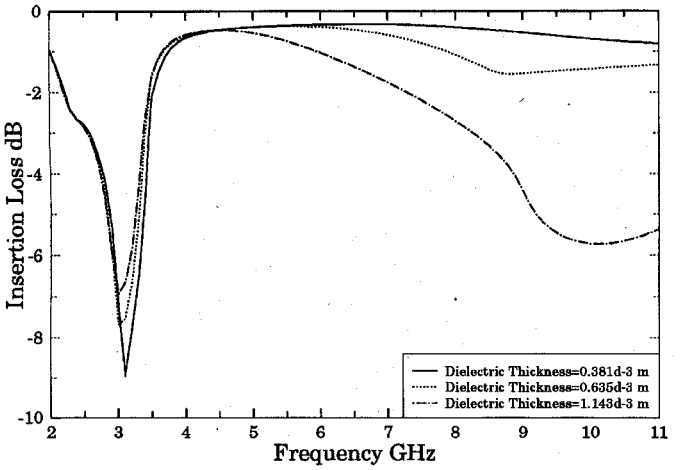

Fig. 13. The effect of the dielectric thickness on the insertion loss ($d_f = 7.62 \times 10^{-4}$ m, $\epsilon_f = 12.0, 4\pi M_s = 2100$ G, $H_{dc} = 700$ Oe, $\Delta H = 80.$ Oe, $R_s = 100\ \Omega, W = 1.016 \times 10^{-2}$ m, $\epsilon_d = 30.0$).

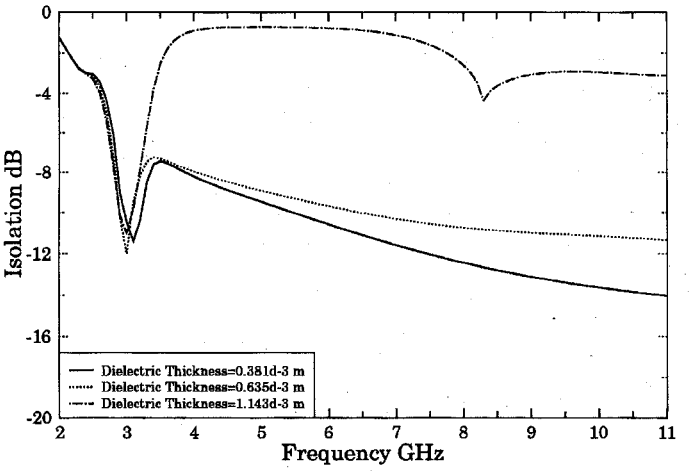

Fig. 14. The effect of the dielectric thickness on the isolation ($d_f = 7.62 \times 10^{-4}$ m, $\epsilon_f = 12.0, 4\pi M_s = 2100$ G, $H_{dc} = 700$ Oe, $\Delta H = 80.$ Oe, $R_s = 100\ \Omega, W = 1.016 \times 10^{-2}$ m, $\epsilon_d = 30.0$).

for the integral to converge. As the subdomain size becomes smaller this upper limit must increase due to the spectral properties of the Fourier transform of the subdomain basis functions. The numerical integration must be performed with enough points to adequately model any rapid changes of the integrand. As the two subdomain basis functions in the integrand become physically farther apart, the integrand becomes more oscillatory requiring more points to assure accurate results. The integrand has poles corresponding to the propagation constants of magnetostatic modes. The integration path is deformed away from the real axis to avoid these poles. The following numerical expressions are used in the course of our simulation:

- maximum integration limit: $\beta_{\max} = C_1/l_{\min}$ and
- number of integration points: $N_i = 1 + [C_2 \Delta\beta_i S_{\max}]$

where

$C_{1,2}$ numerical constants to be determined experimentally;

$l_{\min}$ minimum edge length in the discretization;

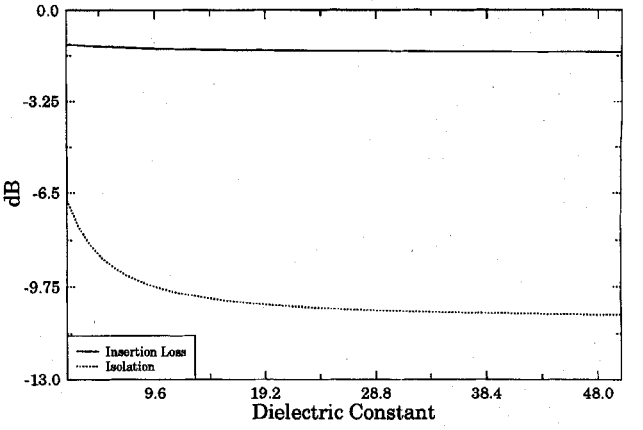

Fig. 15. The effect of the dielectric constant of the dielectric layer on the isolation and the insertion loss, ($d_f = 7.62 \times 10^{-4}$ m, $\epsilon_f = 12.0, 4\pi M_s = 2100$ G, $H_{dc} = 700$ Oe, $\Delta H = 80.$ Oe, $R_s = 100\ \Omega, W = 1.016 \times 10^{-2}$ m, $D_d = 0.381 \times 10^{-3}$ m, Freq. = 6 GHz).

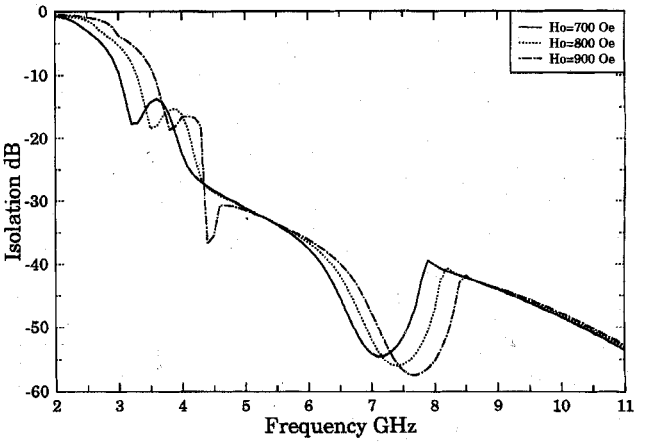

Fig. 16. The effect of the internal dc bias on the isolation, ($d = 7.62 \times 10^{-4}$ m, $\epsilon_f = 12.0, 4\pi M_s = 2100$ G, $\Delta H = 80.$ Oe, $R_s = 100\ \Omega, W = 1.016 \times 10^{-2}$ m).

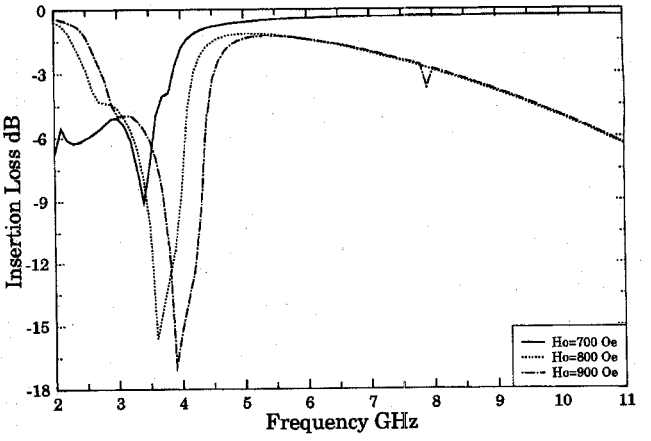

Fig. 17. The effect of the internal dc bias on the insertion loss, ($d = 7.62 \times 10^{-4}$ m, $\epsilon_f = 12.0, 4\pi M_s = 2100$ G, $\Delta H = 80.$ Oe, $R_s = 100\Omega, W = 1.016 \times 10^{-2}$ m).

$S_{\max}$ maximum dimension of the structure;

$\Delta\beta_i$ width of the ith region.

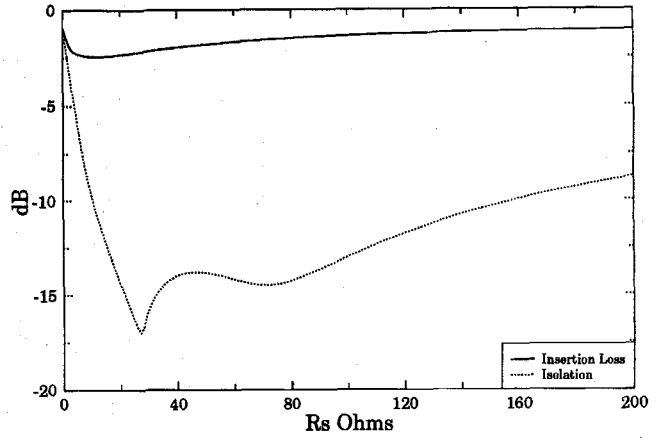

Fig. 18. The effect of the film resistance on the insertion loss and the isolation ($d = 7.62 \times 10^{-4}$ m, $\epsilon_f = 12.0, 4\pi M_s = 1750$ G, $H_{dc} = 800$ Oe, $\Delta H = 80$. Oe, Freq. $= 5$ GH, $W = 1.016 \times 10^{-2}$ m).

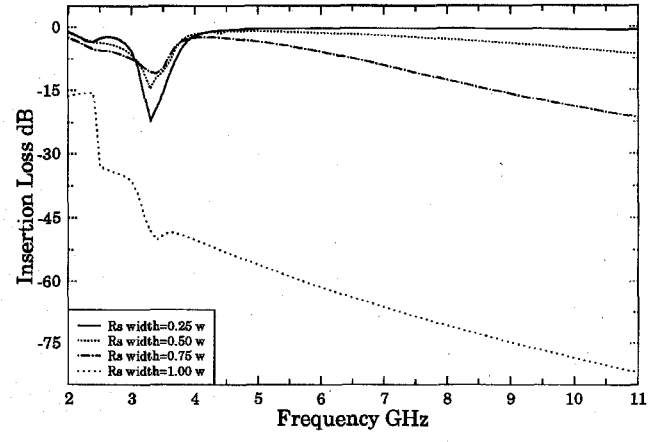

Fig. 19. The effect of the resistive film width on the insertion loss, ($d = 7.62 \times 10^{-4}$ m, $\epsilon_f = 12.0, 4\pi M_s = 2000$ G, $H_{dc} = 700$ Oe, $\Delta H = 80$. Oe, $R_s = 100\ \Omega$, $W = 1.016 \times 10^{-2}$ m).

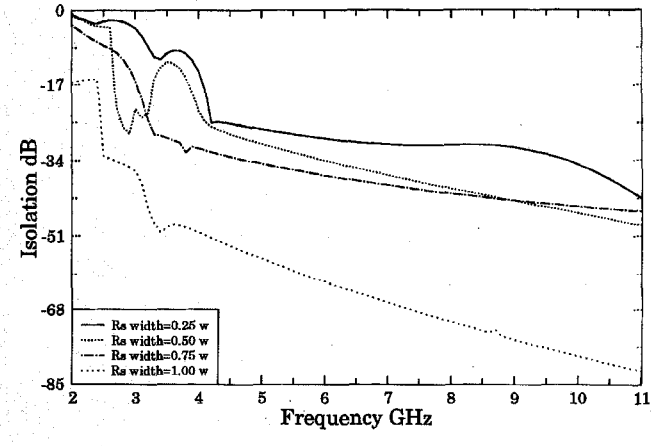

Fig. 20. The effect of the resistive film width on the isolation, ($d = 7.62 \times 10^{-4}$ m, $\epsilon_f = 12.0, 4\pi M_s = 2000$ G, $H_{dc} = 700$ Oe, $\Delta H = 80$. Oe, $R_s = 100\ \Omega$, $W = 1.016 \times 10^{-2}$ m).

III. Numerical Results and Conclusion

We compared our Green's function for the single layer structure shown in Fig. 2 with the Green's function derived by Pozar [13] using the boundary condition method. An excellent agreement between these two methods was achieved.

Since the Green's function of a multilayer structure including a normally biased ferrite substrate is not available in the literature, we compared the limiting case of the ferrite with the Green's function derived by Aberle for multi-layer dielectric structures [14]. Again excellent agreement was achieved.

We constructed a two-dimensional (2-D) MoM code for simulating an EG mode isolator with resistive loading as shown in Fig. 1. First, we examined the limiting case of ferrite with zero ferrite parameters, which is essentially the dielectric case, and compared our results to the widely published results for dielectric microstrip. The computed current distribution in the longitudinal direction over the conductor is shown in Fig. 6. As expected, the current is symmetric. In addition, very good agreement with the dielectric case is obtained for the propagation constant.

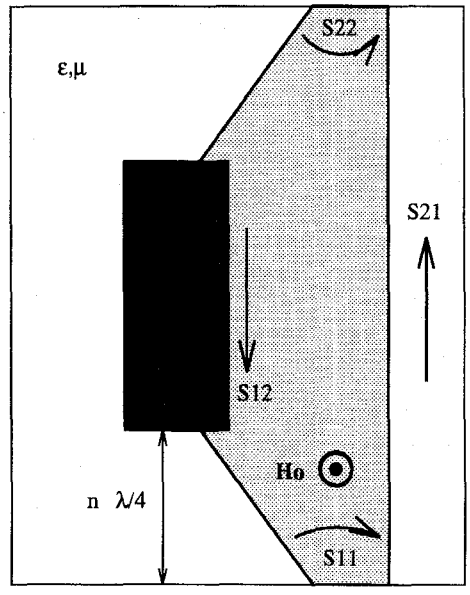

Fig. 21. A 3-D edge-guided isolator with resistive film loading.

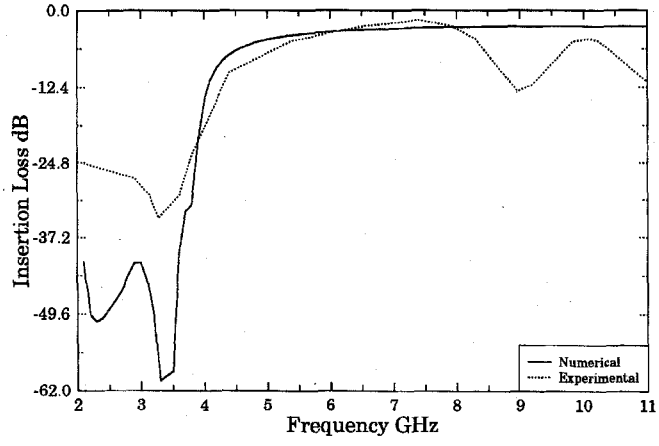

Fig. 22. Comparison between the numerical and experimental insertion loss ($d = 7.62E-04$ m, $\epsilon_f = 12.0, 4\pi M_s = 2100$ G, $H_{dc} = 700$ Oe, $\Delta H = 80$. Oe, $R_s = 100\ \Omega$, $W = 1.016E-2$ m).

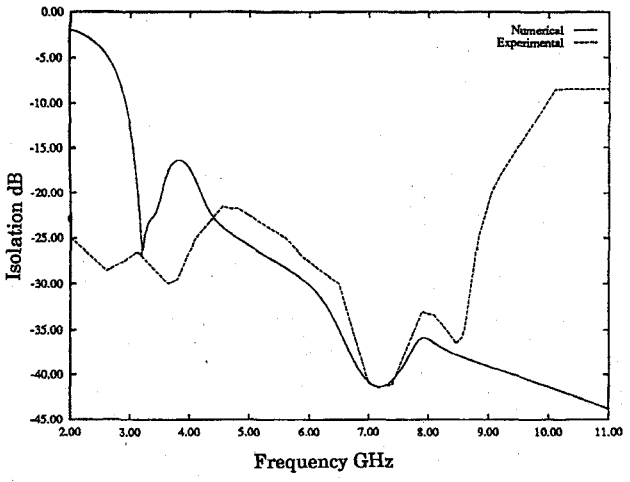

Fig. 23. Comparison between the numerical and experimental isolation ($d = 7.62E-04$ m, $\epsilon_f = 12.0, 4\pi M_s = 2100$ G, $H_{dc} = 700$ Oe, $\Delta H = 80.$ Oe, $R_s = 100\ \Omega, W = 1.016E-2$ m).

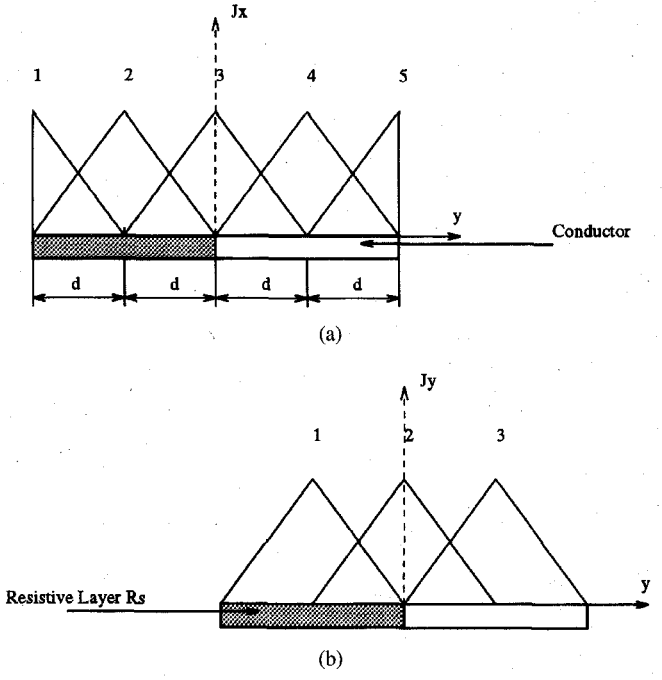

Fig. 24. Current basis functions for (a) longitudinal current (b) transverse current.

For the ferrite case, the asymmetric longitudinal current distribution over the conductor is shown in Fig. 7 for no surface resistance, and in Fig. 8 for a surface resistance equal to 100 Ω over half of the strip. The current distributions shown in Figs. 6–8 are normalized to the highest current value. The phase constants for forward and backward waves are shown in Fig. 9. The computed insertion loss and isolation are given in Fig. 10.

A preliminary analysis of the three isolator structures indicates that the best electrical performance is given by the double-layer structure shown in Fig. 3. While, the performance of the triple-layer structure shown in Fig. 4 is not as good as the other two structures, its advantage is that it can be compatible with MMIC. The insertion loss of the three isolator structures is compared in Fig. 11 and the isolation of the three structures is compared in Fig. 12.

For a single layer of ferrite isolator, the field ellipticities at the upper and the lower boundaries with air counteract each other. If the air at one of these boundaries is replaced by a dielectric layer, as in Figs. 3 and 4, one of the counteracting ellipticities is replaced by a coacting ellipticity which leads to increase in the nonreciprocity and the isolation as well [15]–[17].

The effect of the dielectric thickness of the ferrite-dielectric structure shown in Fig. 3 is studied, the results are given in Figs. 13 and 14. We note that decreasing the dielectric thickness will increase the isolation and decrease the insertion loss which means improving the isolator performance. It is worthwhile to note that the isolation and the insertion loss do not seem to depend significantly on the dielectric constant of the dielectric layer as shown in Fig. 15.

The normally biased ferrite structure excites the magnetostatic forward volume wave which has the frequency range $f_L \geq f \leq f_H$ [18] and [19] where

$$f_L = \gamma H_o$$
$$f_H = \gamma \sqrt{H_o(H_o + 4\pi M_s)}$$

where $H_o, 4\pi M_s$, and γ are the internal bias field, the magnetization of the ferrite, and the gyro-magnetic ratio, respectively. Because of the demagnetization factor for normally biased ferrite, the internal bias field is related to the externally applied field H_e by $H_o = H_e - 4\pi M_s$ [20]. It is shown from Figs. 16 and 17 that the peaks move up in frequency when we increased the internal bias H_o following the limits of the volume wave. The isolation begins after the cutoff limit of the volume wave, f_H.

The optimum resistance of the film is determined from Fig. 18. We note that both the isolation and the insertion loss are equal when the resistance is zero, which is physically true. When the resistance is around 20 times the characteristic impedance of the line, we find that the isolation returns to its value when the resistance is zero. A possible explanation is the high resistance acts like an open circuit and the backward wave will pass through the resistance free region. The insertion loss doesn't depend strongly on the resistance since the forward wave tends to propagates in the resistance free region.

The optimum location and the optimum width of the resistive film are determined from Figs. 19 and 20. The increase of the width of the resistive film will increase the insertion loss and the isolation. When we covered the entire conductor with a resistive film the isolation and insertion loss became equal and the nonreciprocity vanishes. In all of our figures except Figs. 18 and 19, the resistance R_s is on half of the strip, from one edge to its middle. For that reason, the value of R_s does not strongly affect the insertion loss. When R_s covers more than half of the strip, the value of R_s starts to affect the insertion loss.

Finally, we compared our results for the insertion loss and the isolation for the 2-D structure shown in Fig. 1 with the experimental results published in [7] for the structure shown in Fig. 21. Fair agreement is clear from Figs. 22 and 23. The difference between the numerical and the experimental

structures is the difference between Fig. 1 and Fig. 21. In Fig. 1, we assumed matched ports while in Fig. 21 matched ports are assumed only at the center frequency. Thus, the best agreement with the experimental results is in the middle of the frequency range. In addition, in our analysis, the external bias field is assumed to be exactly perpendicular to the substrate which is not necessarily true in the practical case. It is essential to have a flexible tool to be able to handle arbitrarily biased ferrite slab.

APPENDIX A
ELEMENTS OF THE RESISTIVE MATRIX IN SPATIAL DOMAIN

We selected the piece-wise linear subdomain basis function as shown in Fig. 24. The conductor is subdivided into N equal overlapped segments. The elements of the matrices R_{xx} and R_{yy} is found to be

$$R_{xx} = R_s d \begin{bmatrix} \frac{1}{3} & \frac{1}{6} & 0 & 0 & 0 \\ \frac{1}{6} & \frac{2}{3} & \frac{1}{6} & 0 & 0 \\ 0 & \frac{1}{6} & \frac{1}{3} & 0 & 0 \\ 0 & 0 & 0 & 0 & 0 \\ 0 & 0 & 0 & 0 & 0 \end{bmatrix}$$

$$R_{yy} = R_s d \begin{bmatrix} \frac{2}{3} & \frac{1}{6} & 0 \\ \frac{1}{6} & \frac{1}{3} & 0 \\ 0 & 0 & 0 \end{bmatrix}.$$

Similar matrices can be easily derived for a different number of basis function and a different location of the resistance.

REFERENCES

[1] M. E. Hines, "Reciprocal and nonreciprocal modes of propagation in ferrite stripline and microstip devices," *IEEE Trans. Microwave Theory Tech.*, vol. MTT-19, pp. 442–451, May 1971.

[2] G. T. Roome and H. A. Hair, "Thin ferrite devices for microwave integrated circuits," *IEEE Trans. Microwave Theory Tech.*, vol. MTT-16, pp. 411–420, July 1968.

[3] K. Araki, T. Koyama, and Y. Naito, "A new type of isolator using the edge-guided mode," *IEEE Trans. Microwave Theory Tech.*, vol. MTT-23, p. 321, Mar. 1975.

[4] K. Araki, T. Koyama, and Y. Naito, "Reflection problem in a ferrite stripline," *IEEE Trans. Microwave Theory Tech.*, vol. MTT-24, pp. 491–498, Aug. 1976.

[5] M. Dydyk, "One path to wideband isolator design (part i)," *Microwaves*, vol. 16, no. 1, pp. 54–58, Jan. 1977.

[6] ——, "One path to wideband isolator design (part ii)," *Microwaves*, vol. 16, no. 2, pp. 50–56, Feb. 1977.

[7] R. C. Kane and T. Wong, "An edge-guided mode microstrip isolator with transverse slot discontinuity," in *IEEE MTT-S Digest*, pp. 1007–1010, 1990.

[8] *Peripheral Mode Isolator Operates From 3.5 to 11 GHz.* Microwaves, Apr. 1969.

[9] B. Chiron and G. Forterre, "Emploi des ondes de surace electromagnetiques pour la realization de dispositifs gyromagnetiques a tres grande largeur de band," in *Dig. Int. Sem. Microwave Ferrite Devices*, 1972.

[10] M. Blanc, L. Dusson, and J. Guidevoux, "Etude de la fonction isolation a tres large band utilisant des materioux ferrites," in *Dig. Int. Sem. Microwave Ferrite Devices*, 1972.

[11] E. El-Sharawy and R. W. Jackson, "Coplanar waveguide and slot line on magnetic substrates: Analysis and experiment," *IEEE Trans. Microwave Theory Tech.*, vol. 36, pp. 1071–1079, June 1988.

[12] T. F. Elshafiey, J. T. Aberle, and E.-B. A. El-Sharawy, "Green's function formulation for multilayer normally biased ferrite structures using the transmission matrix approach," *IEEE AP Symp. Digest*, vol. AP-S 96, pp. 330–334, July 1996.

[13] D. M. Pozar, "Radiation and scattering characteristics of microstrip antennas on normally biased ferrite substrates," *IEEE Trans. Antennas Propagat.*, vol. 40, pp. 1084–1092, Sep. 1992.

[14] J. T. Aberle, D. M. Pozar, and J. Manges, "Phased arrays of probe-fed stacked microstrip patches," *IEEE Trans. Antennas Propagat.*, vol. AP-42, pp. 920–927, July 1994.

[15] E. El-Sharawy, "Full wave analysis of printed lines on magnetic substrates," Ph.D. dissertation, Univ. Massachusetts, Amherst, 1989.

[16] G. Bock, "New multilayered slot-line structures with high nonreciprocity," *Electron. Lett.*, vol. 19, pp. 966–968, Nov. 1983.

[17] T. I. M. Geshiro, "Analysis of double-layered finlines containing a magnetized ferrite," *IEEE MTT Symp.*, vol. MTT-S 87, pp. 743–744, June 1987.

[18] R. W. Damon and J. R. Eshbach, "Magnetostatic modes of a ferromagnet slab," *J. Appl. Phys.*, vol. 31 supplement, pp. 104S–105S, 1960.

[19] ——, "Magnetostatic modes in a ferrimagnet slab," *J. Phys. Chem. Solids*, vol. 19, no. 3/4, pp. 308–320, 1961.

[20] D. M. Pozar, *Microwave Engineering*. Addison-Wesley, 1990.

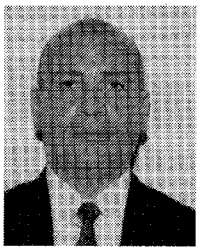

Tarief M. F. Elshafiey (S'92) received the B.S. degree from Military Technical College, Cairo, Egypt, in electrical engineering, the Diploma of Electrophysics from Alexandira University, Alexandria, Egypt, and the M.S. degree from Alexandira University, Alexandira, Egypt. He is currently pursuing the Ph.D. degree in electrical engineering at Arizona State University, Tempe, AZ (ASU).

From 1994 to 1995, he was a Teaching Associate in the electrical engineering department of ASU and he is currently a Research Associate. His research interests include microwave ferrite devices, electromagnetic interactions in layered media, microstrip circuits, and computational electromagnetics.

Mr. Tarief is a member of Eta Kappa Mu.

James T. Aberle (S'81–M'82–SM'92) received the B.S. and M.S. degrees in electrical engineering from Polytechnic Institute of New York (now Polytechnic University), Brooklyn, in 1982 and 1985, respectively, and the Ph.D. degree in electrical engineering from the University of Massachusetts, Amherst, in 1989.

From 1982 to 1985, he was employed by Hazeltine Corporation, Greenlawn, NY, where he worked on the development of wide-band phased array antennas. He was a Graduate Research Assistant at the University of Massachusetts from 1985 to 1989, where he developed and validated computer models for printed antennas. He has been a faculty member at Arizona State University since 1989. During the Summer of 1993, he was a NASA/ASEE Summer Faculty Fellow at NASA Langley Research Center. He is currently an Associate Professor. His research interests include the modeling of complex electromagnetic phenomena.

El-Badawy El-Sharawy (S'86–M'89–SM'92), for a photograph and biography, see this issue, p. 2554.